nature medicine

Molecular imaging of VEGF receptors in angiogenic vasculature with single-chain VEGF-based probes

Marina V Backer[1], Zoya Levashova[2], Vimalkumar Patel[1], Brian T Jehning[1], Kevin Claffey[3], Francis G Blankenberg[2] & Joseph M Backer[1]

We describe a new generation of protein-targeted contrast agents for multimodal imaging of the cell-surface receptors for vascular endothelial growth factor (VEGF). These receptors have a key role in angiogenesis and are important targets for drug development. Our probes are based on a single-chain recombinant VEGF expressed with a cysteine-containing tag that allows site-specific labeling with contrast agents for near-infrared fluorescence imaging, single-photon emission computed tomography or positron emission tomography. These probes retain VEGF activities *in vitro* and undergo selective and highly specific focal uptake into the vasculature of tumors and surrounding host tissue *in vivo*. The fluorescence contrast agent shows long-term persistence and co-localizes with endothelial cell markers, indicating that internalization is mediated by the receptors. We expect that multimodal imaging of VEGF receptors with these probes will be useful for clinical diagnosis and therapeutic monitoring, and will help to accelerate the development of new angiogenesis-directed drugs and treatments.

Preclinical and clinical research indicates that anti-angiogenic drugs can improve the outcome in individuals with tumors. The development of such drugs might be facilitated by the introduction of imaging agents that bind selectively to angiogenic vasculature[1–3]. VEGF receptors, the main target for emerging anti-angiogenic therapies[4,5], are particularly attractive targets for molecular imaging because they are overexpressed in angiogenic endothelium[6–9], accessible directly from the bloodstream, and internalized when they bind VEGF[10], allowing contrast agents to accumulate and be retained.

Most of the VEGF-based imaging agents that have been reported[11–17] are unsuitable for clinical development because of uncertain binding activity of the protein, owing to damage by random radiolabeling[11–13]; unacceptably high liver uptake[14]; or complex probe design[15,16]. As a new approach to the labeling of targeting proteins, we developed a 15-amino-acid humanized fusion tag, named Cys-tag, which contains a unique cysteine for site-specific modification by facile thiol-directed chemistries[17,18]. We found that Cys-tagged dimeric VEGF, site-specifically labeled with technetium-99m (^{99m}Tc), was useful for imaging tumor vasculature[17,18] but was still too complex to be used as a targeting protein. Here, we describe molecular imaging agents based on a new, robust, single-chain Cys-tagged VEGF (scVEGF)[19], a fusion protein that combines two fragments (amino acids 3–112) of human $VEGF_{121}$ cloned head to tail. We show that scVEGF-based imaging agents can be readily prepared for near-infrared fluorescence imaging (NIRF), single-photon emission computed tomography (SPECT) or positron emission tomography (PET) imaging of VEGF receptors in angiogenic vasculature.

RESULTS

Site-specific modification of scVEGF with contrast agents

When we recovered bacterially expressed scVEGF from inclusion bodies and refolded it in a glutathione-containing buffer, a single reactive cysteine appeared only after mild treatment with dithiothreitol (DTT)[19]. To assign this cysteine, we modified DTT-treated scVEGF with Cy5.5-maleimide and cleaved it with BrCN. Fractionation of cleavage products using reverse-phase high-performance liquid chromatography (RP-HPLC) revealed a single Cy5.5-labeled peptide (**Fig. 1a**, circled peak). The N-terminal amino-acid sequence of this peptide (**Fig. 1a**) corresponded to that of Cys-tag. Thus, in spite of the presence of 16 'native' cysteines in scVEGF, mild DTT treatment liberated only the Cys-tag thiol group and made it available for site-specific modification.

We labeled Cys-tag in scVEGF with three agents: a Cy5.5 dye for NIRF imaging, yielding a scVEGF/Cy probe; the ^{99m}Tc chelator hydraziniumpyridine (HYNIC) for SPECT imaging; and a *de novo*–synthesized ^{64}Cu chelator, PEG-DOTA, for PET imaging. The labeled conjugates showed activities similar to those of unmodified scVEGF in two tissue culture assays[17–20]: tyrosine phosphorylation of VEGFR-2, and competition with the chimeric toxin SLT-VEGF for binding to VEGFR-2 (**Fig. 1b,c**). Incubation of scVEGF-PEG-DOTA/^{64}Cu at elevated temperatures (55 °C for 1 h or 95 °C for 20 min), which is essential for chelation of PET radionuclides, did not affect its ability to compete with SLT-VEGF (**Fig. 1c**, for 95 °C treatment). To obtain appropriate controls for nonspecific probe uptake, we inactivated each labeled scVEGF by conjugation of 7 or 8 biotins using *N*-hydroxysuccinimide (NHS) chemistry as described[18]. As expected, biotinylated

[1]SibTech, Inc., 705 North Mountain Road, Newington, Connecticut 06111, USA. [2]Department of Pediatrics & Division of Nuclear Medicine/Department of Radiology & MIPS (Molecular Imaging Program at Stanford), Stanford University, 300 Pasteur Drive, Palo Alto, California 94304, USA. [3]University of Connecticut, Health Center, 263 Farmington Avenue, Farmington, Connecticut 06030, USA. Correspondence should be addressed to J.M.B. (jbacker@sibtech.com).

Received 20 September 2006; accepted 13 November 2006; published online 11 March 2007; doi:10.1038/nm1522

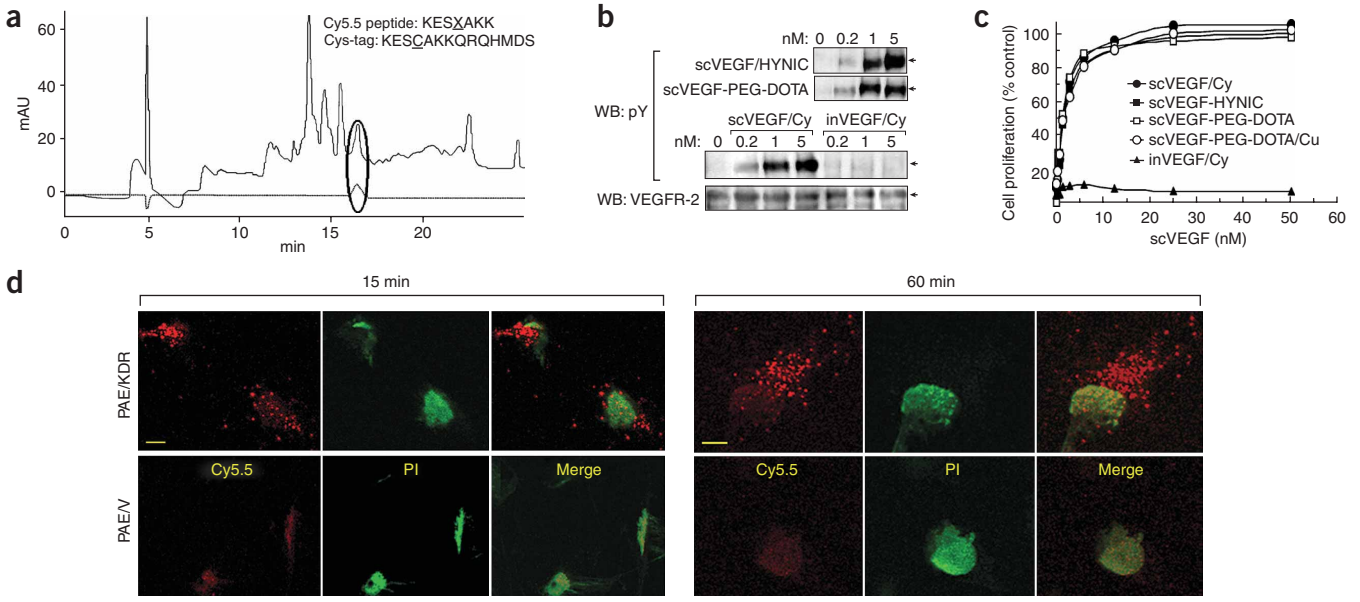

Figure 1 Site-specific modifications do not affect binding and internalization of scVEGF. (**a**) RP-HPLC separation of scVEGF/Cy cleavage products with detection at 280 nm (solid line) and 598 nm (dotted line). Inset: N-terminal sequencing of Cy5.5-labeled peptide circled on the HPLC profile. Peaks around 5 min are of systemic origin. (**b**) Stimulation of VEGFR-2 tyrosine autophosphorylation in 293/KDR cells. Lower panel: blot was stripped and re-probed with antibody for VEGFR-2. InVEGF/Cy, inactivated scVEGF/Cy. WB, western blot. (**c**) Competition with SLT-VEGF in 293/KDR cells. scVEGF conjugated to DOTA was tested before (scVEGF-PEG-DOTA) and after (scVEGF-PEG-DOTA/Cu) incubation at 95 °C for 20 min. (**d**) VEGFR-2 expressing endothelial cells rapidly internalize scVEGF/Cy. Cy5.5, red; propidium iodide (PI), green. Scale bars, 20 μm.

conjugates did not bind to VEGFR-2 (**Fig. 1b,c** for inactivated scVEGF/Cy, called inVEGF/Cy). We further characterized binding of scVEGF-PEG-DOTA/^{64}Cu to 293/KDR cells by Scatchard analysis, which yielded a K_d of 2.8 nM with 1.3×10^6 binding sites per cell (**Supplementary Fig. 1** online). This value is similar to the corresponding values reported for binding of a ^{125}I-VEGF$_{121}$ fusion protein to the same cells[21]. Finally, we tracked the internalization of scVEGF/Cy using confocal microscopy of live porcine aortic endothelial (PAE) cells, either overexpressing VEGFR-2 (PAE/KDR) or lacking the receptor (PAE/V). Only PAE/KDR cells accumulated Cy5.5 in a time-dependent manner, as distinct specks in the perinuclear space (**Fig. 1d**), indicating that labeling of Cys-tag did not prevent VEGFR-2-mediated endocytosis of scVEGF. Together, these data indicate that the functional characteristics of scVEGF were not affected by site-specific modification of Cys-tag.

NIRF imaging with scVEGF/Cy

For NIRF imaging we used luciferase-expressing derivatives of two widely used mammary adenocarcinoma cell lines, mouse 4T1 (ref. 22) and human MDA-MB-231, grown orthotopically in Balb/c and SCID/NCr mice, respectively. The borders of these tumors were readily defined by bioluminescence imaging (BLI), providing a framework for assignment of NIRF images obtained with scVEGF/Cy.

To confirm the selectivity of scVEGF/Cy binding *in vivo*, we first tested functionally inactive inVEGF/Cy, and found no evidence of its uptake in the tumor areas defined by BLI (**Fig. 2a**). By contrast, functionally active scVEGF/Cy selectively accumulated in BLI-defined areas, indicating that binding to VEGF receptors was crucial for imaging (**Fig. 2a**, scVEGF/Cy panels). Selective accumulation of scVEGF/Cy could be detected in barely palpable tumors, indicating that imaging of VEGF receptors might be particularly useful for detecting small primary tumors and metastatic lesions. The pattern of scVEGF/Cy accumulation was highly heterogeneous, as has been reported for all molecular imaging probes that target endothelial cell markers[1–3,11–17]. Injection of scVEGF/Cy together with a tenfold excess of unlabeled scVEGF resulted in a markedly weaker NIRF image (data not shown). The intensity of NIRF images persisted for several hours after scVEGF/Cy injection and remained nearly constant for at least 7 d after injection, whereas the tumors continued to grow over the area of the probe uptake (**Supplementary Figs. 2** and **3** online).

As clearance of radiolabeled VEGF-based probes occurs within around 1 h (refs. 16,18), persistent Cy5.5 fluorescence within the tumor area could be best explained by internalization of scVEGF/Cy by receptor-mediated endocytosis and entrapment of highly charged Cy5.5 inside cells. For both tumor models, Cy5.5 fluorescence co-localized with immunofluorescence staining for VEGFR-2, (**Fig. 2b**, for 4T1luc tumors), which, in turn, co-localized with a pan-endothelial marker, CD31 (data not shown). Some areas had low Cy5.5 fluorescence, however, reflecting the heterogeneity of scVEGF/Cy accumulation, in spite of the presence of VEGFR-2 (**Fig. 2c**).

Hypothetically, scVEGF/Cy could accumulate as a result of enhanced endocytic activity of tumor endothelial cells. We therefore tested whether an unrelated growth factor can target Cy5.5 to the tumor endothelium. For these experiments, we engineered a Cys-tagged epidermal growth factor, site-specifically labeled it with Cy5.5-maleimide and tested it in the 4T1 tumor model. Although the label accumulated in the tumor, Cy5.5 fluorescence did not co-localize with CD31 (**Supplementary Fig. 4** online).

Our NIRF experiments showed that the areas of enhanced scVEGF/Cy uptake were consistently extended beyond BLI-defined tumor areas in both the 4T1luc and MDA-231luc models (**Fig. 2b**, **Supplementary Figs. 2** and **3** online). As BLI depends on the uptake and metabolism of luciferin and does not necessarily mark the exact histological margins of the tumor, this effect might be an artifact. As tumors are

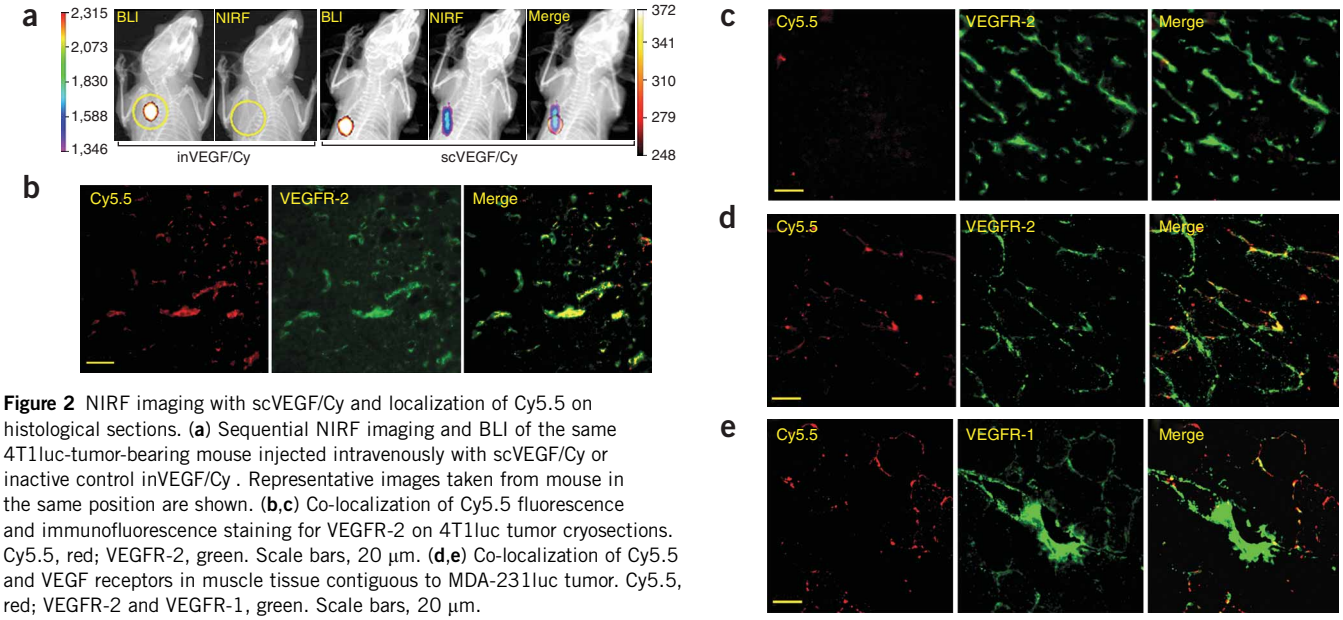

Figure 2 NIRF imaging with scVEGF/Cy and localization of Cy5.5 on histological sections. (**a**) Sequential NIRF imaging and BLI of the same 4T1luc-tumor-bearing mouse injected intravenously with scVEGF/Cy or inactive control inVEGF/Cy . Representative images taken from mouse in the same position are shown. (**b**,**c**) Co-localization of Cy5.5 fluorescence and immunofluorescence staining for VEGFR-2 on 4T1luc tumor cryosections. Cy5.5, red; VEGFR-2, green. Scale bars, 20 μm. (**d**,**e**) Co-localization of Cy5.5 and VEGF receptors in muscle tissue contiguous to MDA-231luc tumor. Cy5.5, red; VEGFR-2 and VEGFR-1, green. Scale bars, 20 μm.

known to induce changes in the surrounding host vasculature[23], however, we hypothesized that such tumor-host interactions might be responsible for the accumulation of scVEGF beyond the margins of the tumors. Co-localization analysis of serial cryosections containing both tumor and surrounding muscle tissue revealed Cy5.5 fluorescence in endothelial capillary cells between large, well-defined muscle cells (**Fig. 2d**,**e**). In these areas, Cy5.5 fluorescence co-localized with immunofluorescence staining for both VEGFR-2 and VEGFR-1, indicating that both receptors might be responsible for the uptake of scVEGF/Cy in tumor-activated host vasculature.

SPECT imaging with scVEGF/Tc

We used ^{99m}Tc to radiolabel scVEGF-HYNIC and its inactivated analog, yielding scVEGF/Tc and inVEGF/Tc, respectively. Both tracers were >95% cleared from the circulation within 50 min of intravenous injection (**Fig. 3a**, for scVEGF/Tc). To characterize the stability of scVEGF/Tc in the circulation, we obtained plasma from blood collected 3 and 50 min after the injection and precipitated scVEGF/Tc with the soluble VEGF receptor KDR-Fc from plasma aliquots containing the same amounts of radioactivity. Western blot analysis showed that similar amounts of scVEGF were collected from both plasma samples, indicating that circulating scVEGF/Tc remained stable and capable of binding VEGF receptors until >95% of the tracer had been cleared from the blood (**Supplementary Fig. 5** online, upper row).

The biodistribution of scVEGF/Tc in mice bearing 4T1luc tumors (**Fig. 3b**) was similar to those of a binary ^{99m}Tc-adaptor/VEGF non-covalent complex[16] and site-specifically labeled dimeric VEGF (ref. 18). The relatively high kidney and liver uptake, as with other HYNIC-labeled proteins, was probably the result of slow lysosomal clearance of the radiolabeled metabolites, such as $(\text{tricine})_2$-^{99m}Tc-HYNIC-amino acid or $(\text{tricine})_2$-^{99m}Tc-HYNIC-oligopeptide[24,25].

SPECT imaging showed highly heterogeneous focal accumulation of scVEGF/Tc in the tumor area. This accumulation was considerably greater than that of inVEGF/Tc (**Fig. 3c**). Region of interest (ROI) analysis indicated that the uptake of scVEGF/Tc at the tumor rim was 10–15 times higher than in the soft-tissue background; this contrasts with the nearly uniform low uptake of inVEGF/Tc (**Fig. 3c** and **Supplementary Fig. 6** online). Subsequent autoradiography of cryosections from harvested tumors and contralateral pectoralis muscle confirmed the selective and predominately peripheral accumulation of scVEGF/Tc only within tumor tissue (**Fig. 3d**).

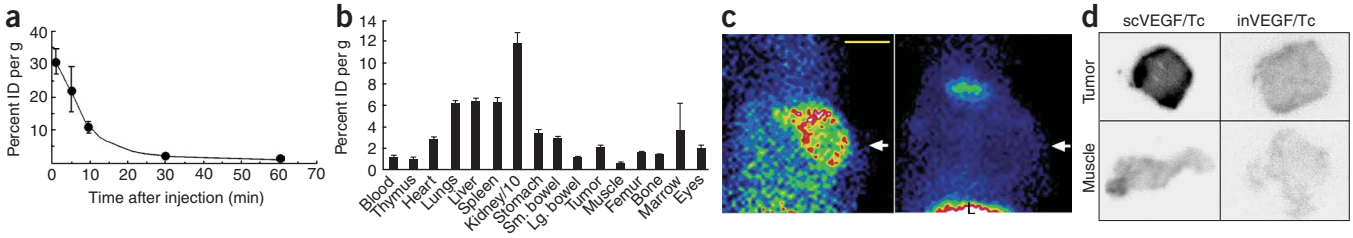

Figure 3 Blood clearance, biodistribution and SPECT imaging of scVEGF/Tc. (**a**,**b**) Blood clearance (**a**) and biodistribution (**b**) of radioactivity 1 h after intravenous injection of scVEGF/Tc. Sm. and Lg. bowel, small and large bowel, respectively. ID, injected dose. (**c**) SPECT imaging. Serial frontal images of two separate 4T1luc-tumor-bearing mice taken 1 h after injection of scVEGF/Tc (left) or inVEGF/Tc (right). Arrows indicate tumor positions. L, liver rim; white is the highest activity in false color images. Scale bar, 1 cm. (**d**) Autoradiographs of cryosections of tumors and normal pectoralis muscle from the contralateral chest wall removed immediately after *in vivo* imaging.

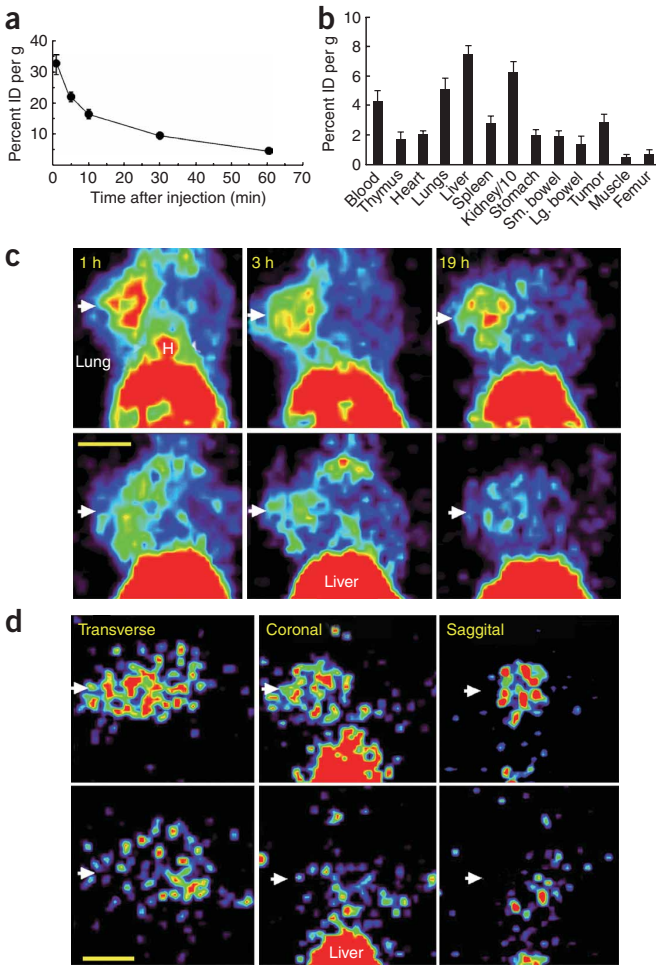

Figure 4 Blood clearance, biodistribution and PET imaging of scVEGF/Cu. (**a**,**b**) Blood clearance (**a**) and biodistribution (**b**) of radioactivity 2 h after injection with scVEGF/Cu. (**c**) PET imaging. Serial frontal images of two mice bearing 4T1luc tumors in the left axillary fat pads 1, 3 and 19 h after injection of either 100 μCi scVEGF/Cu (top row) or equivalent amounts of inVEGF/Cu (bottom row). White arrows mark left mammary fat pad tumor in each image. H, heart or blood pool activity observed at 1 h. Scale bar, 1 cm. (**d**) Representative transverse, coronal and sagittal tomographic slices through the left mouse mammary fat pad tumor taken 2 h after injection of 6.25 μCi of free (upper row) or KDR-Fc-bound scVEGF/Cu (lower row). White arrows mark the left mammary fat pad tumor. Scale bar, 1 cm.

PET imaging with scVEGF/Cu

We used ^{64}Cu to label scVEGF-PEG-DOTA and its inactivated analog, yielding scVEGF/Cu and inVEGF/Cu, respectively. As expected, because of incorporation of the PEG linker between DOTA and scVEGF, scVEGF/Cu showed considerably prolonged blood clearance (**Fig. 3a**), as compared with scVEGF directly conjugated to DOTA (data not shown) or scVEGF/Tc (**Fig. 4a**). The stability in the circulation tested by KDR-Fc precipitation as described above (**Supplementary Fig. 5** online) indicated that scVEGF/Cu was stable and intact until blood clearance of at least 95% of the activity. We tested the stability of scVEGF/Cu in plasma *ex vivo* for times beyond 1 h (**Supplementary Fig. 7** online) and found that less than 5% of ^{64}Cu was released from protein complexes even after 5 h of incubation at 37 °C, either in pooled mouse plasma or in radiolabeling buffer.

The biodistribution of scVEGF/Cu showed half as much renal accumulation of the tracer as compared with scVEGF/Tc (**Fig. 4b**, compare with **Fig. 3b**), a distinct advantage with respect to the relative radiation dose to the kidneys. More importantly, scVEGF/Cu also delivered more tracer to the tumor (**Fig. 4b**, compare with **Fig. 3b**). As our NIRF imaging results indicated that scVEGF-based probes were internalized and that the imaging agent remained sequestered for a long time after clearance, we performed serial PET imaging of mice bearing 4T1luc tumors 1, 3 and 19 h after injection of either scVEGF/Cu (**Fig. 4c**, top row) or inVEGF/Cu (**Fig. 4c**, lower row). Persistent focal accumulation of scVEGF/Cu in the tumor area was substantially higher and more heterogeneous than that of inVEGF/Cu, and the difference was greatest after 19 h (**Fig. 4c**). To confirm that accumulation of scVEGF/Cu was receptor mediated, we preincubated scVEGF/Cu with KDR-Fc before injection, and used the same amounts of KDR-Fc-bound and free scVEGF/Cu for PET imaging. Preincubation with KDR-Fc greatly reduced the accumulation of scVEGF/Cu in the tumor area (**Fig. 4d**).

DISCUSSION

Our data indicate that scVEGF is a robust targeting protein that allows the development of molecular imaging agents for different imaging modalities through facile thiol-directed chemistries. The use of VEGF-based imaging might raise concerns about a potential pro-angiogenic outcome. Although a definitive answer to these concerns requires extensive experimentation, we expect that injection of small amounts of the protein for diagnostic imaging will cause no adverse effects[26]. In addition, it has been reported that endogenous expression of a VEGF fragment containing amino acids 1–113 does not stimulate tumor growth and, in fact, can inhibit angiogenesis[27]. In view of these data, we expect that scVEGF, which combines two fragments consisting of amino acids 3–112 of the protein, would be unlikely to induce angiogenesis or secondary tumors, especially at the tracer dosages needed for imaging.

Imaging by NIRF, SPECT and PET shows that scVEGF-based agents bind to and are internalized by VEGF receptors in the tumor area. Nevertheless, low but detectable accumulation of inactivated or KDR-Fc-bound scVEGF/Cu probe in the tumor area indicates that nonspecific mechanisms might also contribute to accumulation within the tumor. Further experiments are required to establish whether nonspecific mechanisms also contribute to imaging with scVEGF-based probes, or whether they are completely superseded by receptor-mediated uptake.

Judging by co-registered NIRF and BLI images, the scVEGF/Cu uptake area includes contiguous host vasculature, where sequestered Cy5.5 is found in host capillary endothelial cells. As activation of host vasculature is induced by very small growing tumor lesions[25], investigation is warranted to establish whether diagnostic imaging with scVEGF-based probes could improve detection of such lesions.

The accumulation and retention of all scVEGF-based probes in the tumor area is highly heterogeneous, and several mechanisms (for example, non-uniform perfusion of tumor vasculature, differential receptor occupancy by host VEGF or differential accessibility of VEGF receptors on luminal and subluminal surfaces of the endothelium) might be responsible for this effect. As the clinical value of scVEGF-based imaging agents will depend to a great extent on their ability to characterize the prevalence of VEGF receptors, this issue should be addressed in future research.

In summary, angiogenesis is and will remain an important therapeutic target that is suitable for complex and personalized treatment regimens[28–31]. We expect that molecular imaging of VEGF receptors with scVEGF-based agents will facilitate progress in this area.

METHODS

Tissue culture. We stably transfected 4T1 (ATCC no. CRL-2539) and MDA-MB-231 (ATCC no. HTB-26) cells with the pGL3 (Promega) and pcDNA/Zeo (Invitrogen) plasmids and clonally selected them on zeocin (0.5 mg ml^{-1}). We designated the clones with the highest luciferase activity 4T1luc and MDA-231luc, respectively. 293/KDR and PAE/KDR cells expressing full-length human VEGFR-2, 293/KDR-Fc cells expressing soluble VEGFR-2 (KDR-Fc), and PAE/V cells have been described previously[21]. We performed VEGFR-2 autophosphorylation and competition with SLT-VEGF as described[17–20].

Cell microscopy. We incubated PAE/KDR and PAE/V cells with 10 nM scVEGF/Cy at 37 °C, washed them extensively with PBS and then with 0.5 M NaCl in PBS, mounted them in culture medium with 2 μM propidium iodide (Sigma) and imaged them immediately using a confocal laser scanning microscope (Olympus FV1000; Olympus America).

Animals. We gave BALB/c and SCID/NCr (BALB/c background) mice (5–6 weeks old, Charles River Laboratories) 4T1luc cells (5×10^3 cells per mouse) and MDA-231luc cells (5×10^6 cells per mouse), respectively, in the fat pad regions. The protocol for the animal studies was approved by the Institutional Animal Care and Use Committees at the University of Connecticut Health Center and at Stanford University.

NIRF imaging. We treated scVEGF with DTT as described[19], mixed it with a fivefold molar excess of Cy5.5-maleimide (GE Healthcare), incubated it for 1.5 h and desalted it. We separated free scVEGF on a Q-column (GE Healthcare) and calculated the extent of modification from RP-HPLC peak intensities (C4 Alltech Macrosphere) at 216 nm for protein and 598 nm for Cy5.5. For NIRF and BLI, we gave mice scVEGF/Cy (10 μg per mouse) intravenously; 5 min later, luciferin (0.5 mg per mouse) intraperitoneally; and 5 min later, a mixture of ketamine (120 mg kg^{-1}) and xylazine (8 mg kg^{-1}) intramuscularly. We obtained images on a Kodak Image Station 4000 Multi-Modal Imaging System (IS4000MM) equipped with an X-ray unit and on a Kodak Image Station 2000.

N-terminal sequencing. scVEGF conjugates were completely denatured with a 100-fold molar excess of Tris(2-carboxyethyl)phosphine (Pierce) at 65 °C for 1 h followed by a 30-min incubation with a 1,000-fold excess of iodacetamide, then digested with BrCN (60-fold molar excess) for 16 h in 70% formic acid. We analyzed peptide fragments separated by RP-HPLC (C4 column) by N-terminal sequencing at Yale Cancer Center Mass Spectrometry Resources at the W. M. Keck Foundation Biotechnology Resource Laboratory.

Immunofluorescence. We fixed tumor 7-μm-thick cryosections with 1% formaldehyde (Polysciences) and blocked them with an avidin-biotin blocking kit (Molecular Probes) followed by blocking with 5% appropriate normal serum. Antibodies for VEGFR-2(KDR/Flk-1) and CD31(PECAM) were from Pharmingen; antibody for VEGFR-1(Flt-1) was from NeoMarkers. We coupled biotinylated second antibodies to streptavidin-peroxidase conjugate and visualized them by AlexaFluor-488 using tyramine amplification technique (TSA HRP-streptavidin Kit, Molecular Probes). We observed and digitized images on a Zeiss LSM 510 microscope using a ×43 oil objective.

SPECT imaging. We conjugated HYNIC-maleimide to scVEGF and radiolabeled it with ^{99m}Tc as described[16,18] to an activity of 25 μCi per μg protein for clearance and biodistribution (0.1 mCi per mouse, $n = 4$) and 160 μCi per μg for SPECT imaging (1–1.2 mCi per mouse, $n = 5$). We performed blood clearance, biodistribution and SPECT imaging as described[16,18].

PET imaging. We mixed NHS-PEG-maleimide (Nektar Therapeutics) with a fivefold molar excess of 2-(4-aminobenzyl)-DOTA (1,4,7,10-tetraazacyclododecane-1,4,7,10-tetraacetic acid, Macrocyclic) in carbonate buffer pH 8.0 and incubated it for 1 h. After quenching of unreacted NHS (0.1 M Tris-HCl, pH 8.0, 30 min), we added deprotected scVEGF to a final protein-to-DOTA molar ratio of 1:10, incubated for 1 h, and then carried out RP-HPLC purification on a preparative C4 Vydac column. We incubated 20 μg of conjugate with 400–500 μCi of ^{64}Cu (Washington University Medical School) in 0.1 M sodium acetate (pH 5.5) for 1 h at 55 °C, sequestered residual ^{64}Cu by 1 mM EDTA, and removed it by desalting, yielding 40% efficiency of scVEGF-PEG-DOTA radiolabeling. We gave two groups of tumor-bearing mice ($n = 6$) 2–5 μCi per mouse intravenously for biodistribution studies or 100 μCi per mouse intravenously for PET imaging. To sequester scVEGF, we mixed scVEGF/Cu (6.25 μCi, 1.25 μg) with a fivefold molar excess of recombinant human soluble VEGFR-2/KDR-Fc (R&D Systems) in 0.1 M Tris-HCl, pH 8.0, 0.15 M NaCl and 0.1% BSA, and incubated it for 2 h at 4 °C before injection. We incubated control scVEGF/Cu (6.25 μCi, 1.25 μg) under the same conditions without soluble VEGFR-2. We obtained 10-min static scans of mice in a prone position on a microPET R4 rodent model scanner (Concorde Microsystems) equipped with computer-controlled vertical and horizontal bed motion, with an effective axial field of view (FOV) of 7.8 cm and a transaxial FOV of 10 cm. We placed mice anesthetized with 2% isoflurane near the center of the FOV to ensure the highest image resolution and sensitivity. We reconstructed the images by a two-dimensional, ordered-subsets expectation maximum algorithm. No correction was necessary for attenuation and scattering. We obtained relative tumor or organ radioactivity concentrations from mean pixel values within the multiple ROI volumes.

Note: Supplementary information is available on the Nature Medicine website.

ACKNOWLEDGMENTS

We thank J. Pizzonia (KODAK Molecular Imaging Systems) for help with NIRF imaging; K. Tracht (Olympus America) for help with microscopy; P.T. Pienkos (Molecular Logix) for codon optimized human EGF; and R. Barth (The Ohio State University) for F98-EGFR(F) cells. This work was supported in part by NIH grants R43 CA113080 and R21 EB001946 to J.M.B., NIH 1 P50 CA114747 to F.G.B., and by support from NIH CA064436 and the Patrick and Catharine Weldon Donaghue Foundation to K.P.C.

AUTHOR CONTRIBUTIONS

M.V.B. and Z.L. contributed equally to this manuscript. M.V.B., F.G.B. and J.M.B. conceived of and initiated the project, coordinated discovery research and wrote the manuscript; M.V.B. designed imaging conjugates, validated all probes in tissue culture and performed colocalization studies; M.V.B. and J.M.B. designed and conducted optical imaging experiments; Z.L. and F.G.B. prepared radiolabeled SPECT and PET probes and performed all experiments with these probes; V.P. and B.T.G. made scVEGF-based conjugates; and K.C. performed confocal microscopy experiments. All authors discussed and commented on the manuscript.

COMPETING INTERESTS STATEMENT

The authors declare competing financial interests: details accompany the full-text HTML version of the paper at www.nature.com/naturemedicine/.

Published online at http://www.nature.com/naturemedicine
Reprints and permissions information is available online at http://npg.nature.com/reprintsandpermissions

1. Miller, J.C. *et al.* Imaging angiogenesis: applications and potential for drug development. *J. Natl. Cancer Inst.* **97**, 172–187 (2005).
2. Haubner, R. & Wester, H.J. Radiolabeled tracers for imaging of tumor angiogenesis and evaluation of anti-angiogenic therapies. *Curr. Pharm. Des.* **10**, 1439–1455 (2004).
3. Wu, Y. *et al.* microPET imaging of glioma integrin $\alpha_v\beta3$ expression using (64)Cu-labeled tetrameric RGD peptide. *J. Nucl. Med.* **46**, 1707–1718 (2005).
4. Ferrara, N., Gerber, H.P. & LeCouter, J. The biology of VEGF and its receptors. *Nat. Med.* **9**, 669–676 (2003).
5. Manley, P.W. *et al.* Advances in the structural biology, design and clinical development of VEGF-R kinase inhibitors for the treatment of angiogenesis. *Biochim. Biophys. Acta* **1697**, 17–27 (2004).
6. Couffinhal, T. *et al.* Vascular endothelial growth factor/vascular permeability factor (VEGF/VPF) in normal and artherosclerotic human arteries. *Am. J. Pathol.* **150**, 1673–1685 (1997).
7. Koukourakis, M.I. *et al.* Vascular endothelial growth factor/KDR activated microvessel density versus CD31 standard microvessel density in non-small cell lung cancer. *Cancer Res.* **60**, 3088–3095 (2000).
8. Witmer, A.N. *et al.* Expression of vascular endothelial growth factor receptors 1, 2, and 3 in quiescent endothelia. *J. Histochem. Cytochem.* **50**, 767–777 (2002).
9. Vajkoczy, P. *et al.* Microtumor growth initiates angiogenic sprouting with simultaneous expression of VEGF, VEGF receptor-2, and angiopoietin-2. *J. Clin. Invest.* **109**, 777–785 (2002).
10. Bikfalvi, A. *et al.* Interaction of vasculotropin/vascular endothelial cell growth factor with human umbilical vein endothelial cells: binding, internalization, degradation, and biological effect. *J. Cell. Physiol.* **149**, 50–59 (1991).

11. Li, S. *et al.* Characterization of ^{123}I-vascular endothelial growth factor-binding sites expressed on human tumour cells: possible implication for tumour scintigraphy. *Int. J. Cancer* **91**, 789–796 (2001).
12. Li, S. *et al.* Imaging gastrointestinal tumours using vascular endothelial growth factor-165 (VEGF165) receptor scintigraphy. *Annals Oncol.* **14**, 1274–1277 (2003).
13. Li, S. *et al.* Iodine-123-vascular endothelial growth factor-165 (123I-VEGF165). Biodistribution, safety and radiation dosimetry in patients with pancreatic carcinoma. *Q. J. Nucl. Med. Mol. Imag.* **48**, 198–206 (2004).
14. Lu, E. *et al.* Targeted *in vivo* labeling of receptors for vascular endothelial growth factor: approach to identification of ischemic tissue. *Circulation* **108**, 97–103 (2003).
15. Chan, C. *et al.* A human transferrin(hnTf)-VEGF fusion protein containing an integrated binding site for 111In for imaging tumor angiogenesis. *J. Nucl. Med.* **46**, 1745–1752 (2005).
16. Blankenberg, F.G. *et al.* Tumor imaging using a standardized radiolabeled adapter protein docked to vascular endothelial growth factor (VEGF). *J. Nucl. Med.* **45**, 1373–1380 (2004).
17. Backer, M.V. *et al.* Vascular endothelial growth factor selectively targets boronated dendrimers to tumor vasculature. *Mol. Cancer Ther.* **4**, 1423–1429 (2005).
18. Blankenberg, F.G. *et al. In vivo* tumor angiogenesis imaging with site-specific labeled ^{99m}Tc-HYNIC-VEGF. *Eur. J. Nucl. Med. Mol. Imag.* **33**, 841–848 (2006).
19. Backer, M.V., Patel, V., Jehning, B.T., Claffey, K. & Backer, J.M. Surface immobilization of active vascular endothelial growth factor via a cysteine-containing tag. *Biomaterials* **27**, 5452–5458 (2006).
20. Backer, M.V. & Backer, J.M. Targeting endothelial cells overexpressing VEGFR-2: selective toxicity of shiga-like toxin-VEGF fusion proteins. *Bioconjugate Chem.* **12**, 1066–1073 (2001).
21. Backer, M.V. & Backer, J.M. Functionally active VEGF fusion proteins. *Prot. Exp. Purif.* **23**, 1–7 (2001).
22. Heppner, G.H. *et al.* Nontransgenic models of breast cancer. *Breast Cancer Res.* **2**, 331–334 (2000).
23. Li, C.Y. *et al.* Initial stages of tumor cell-induced angiogenesis: evaluation via skin window chambers in rodent models. *J. Natl. Cancer Inst.* **92**, 143–147 (2000).
24. Ono, M. *et al.* Intracellular metabolic fate of radioactivity after injection of technetium-99m-labeled hydrazino nicotinamide derivatized proteins. *Bioconjugate Chem.* **10**, 386–394 (1999).
25. Ono, M. *et al.* Control of radioactivity pharmacokinetics of 99mTc-HYNIC-labeled polypeptides derivatized with ternary ligand complexes. *Bioconjugate Chem.* **13**, 491–501 (2002).
26. Zhang, W. *et al.* A monoclonal antibody that blocks VEGF binding to VEGFR2 (KDR/Flk-1) inhibits vascular expression of Flk-1 and tumor growth in an orthotopic human breast cancer model. *Angiogenesis* **5**, 35–44 (2002).
27. Lee, S. *et al.* Processing of VEGF-A by matrix metalloproteinases regulates bioavailability and vascular patterning in tumors. *J. Cell Biol.* **169**, 681–691 (2005).
28. Jain, R.K. Normalization of tumor vasculature: an emerging concept in antiangiogenic therapy. *Science* **307**, 58–62 (2005).
29. McCarty, M.F. *et al.* Promises and pitfalls of anti-angiogenic therapy in clinical trials. *Trends Mol. Med.* **9**, 53–58 (2003).
30. Kerbel, R.S. & Kamen, B.A. The anti-angiogenic basis of metronomic chemotherapy. *Nat. Rev. Cancer* **4**, 423–436 (2004).
31. Jain, R.K. *et al.* Lessons from phase III clinical trials on anti-VEGF therapy for cancer. *Nature Clin. Practice Onc* **3**, 24–40 (2006).

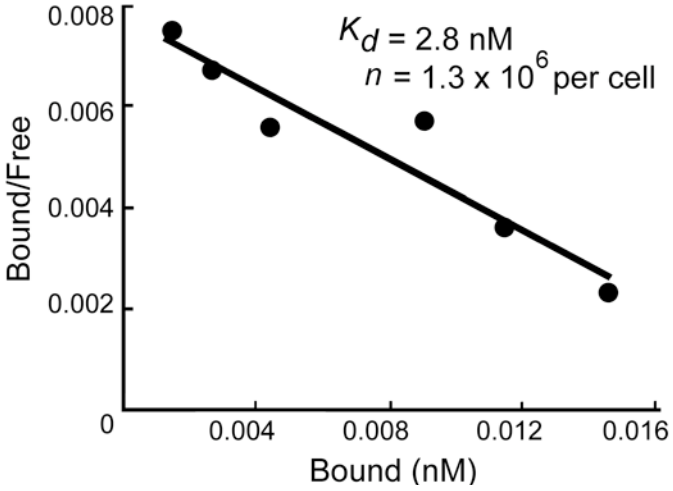
K_d = 2.8 nM
n = 1.3 x 10^6 per cell
Bound/Free
0.008
0.006
0.004
0.002
0
0.004
0.008
0.012
0.016
Bound (nM)

Supplementary Figure 1. Scatchard analysis of scVEGF/Cu binding to VEGFR-2 on 293/KDR cells.

Cells were grown on 12-well plates under normal culture conditions to near-confluence, and shifted to serum-free medium at room temperature. After a 45-min incubation at room temperature, varying amounts of scVEGF/Cu were added to cells in triplicate wells, and incubation was continued for 90 min, followed by two PBS and one high-salt (0.5 M NaCl in PBS) wash. Cells we lysed in a buffer containing 10 mM Tris HCl pH 8.0, 1% Triton X-100 and 0.25 M NaCl counted in Perkin-Elmer Cobra II Auto-gamma counter. A number of cells per well was determined by counting cells from triplicate control wells after all washes. Non-specific binding was determined for the same amounts of scVEGF/Cu supplemented with 100-fold molar excess of non-radiolabled scVEGF-PEG-DOTA, which was passed through conditions of ^{64}Cu loading. Calculated K*d* and a number of binding sites per cell (*n*) are indicated.

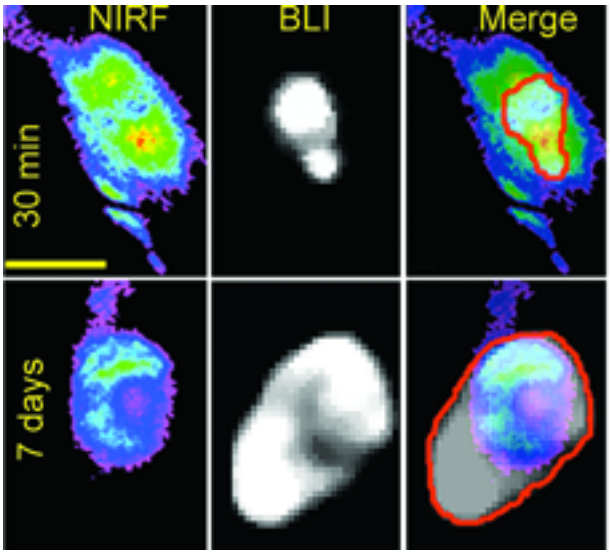
NIRF
BLI
Merge
30 min
7 days

Supplementary Figure 2. Long-term retention of Cy5.5 after imaging with scVEGF/Cy. 4T1luc tumor-bearing mice (*n*=5) were injected with scVEGF/Cy and imaged daily for 7 days. Fresh luciferin was injected prior to each imaging. Representative first (30 min post-injection) and last (7 days post-injection) NIRF and BLI images for the same mouse are presented. On merged BLI and NIRF images the BLI footprint is contoured in red. Note that despite an average 4.5-fold increase in the tumor size, as judged by caliper measurements (from 6 x 5 x 2 mm (length x width x height) to 11 x 7 x 3 mm, average measurements) and BLI footprints, the intensity and the NIRF image area did not change significantly (ROI area ~110,000 px, ROI intensity ~280,000). Scale bar, 1 cm.

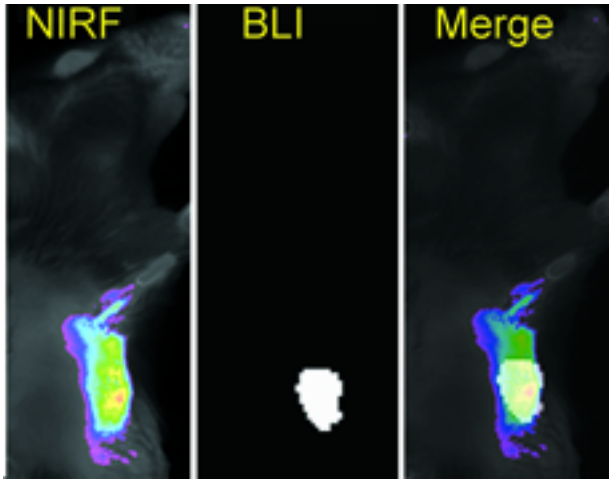
NIRF
BLI
Merge

Supplementary Figure 3. NIRF imaging with scVEGF/Cy in MDA-231luc orthotopic tumor model.

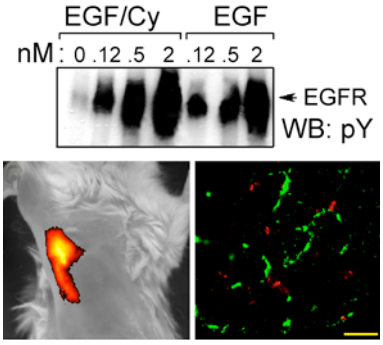
EGF/Cy
EGF
nM: 0 .12 .5 2 .12 .5 2
EGFR
WB: pY

Supplementary Figure 4. Functionally active Cys-EGF/Cy accumulates in tumor area, but does not co-localize with endothelial cells

Codon optimized human EGF was cloned in pET/Hu-R4C(G_4S) vector[17] for expression with an N-terminal Cys-tag. The resulting Cys-tagged EGF was expressed in *E. coli*, deprotected and modified with Cy5.5-maleimide site-specifically as described for scVEGF. Stimulation of EGFR tyrosine autophosphorylation on F98-EGFR(F) rat glioma cells (top) was done as described for VEGFR-2 phosphorylation assay[17-20]. Stimulation with human EGF (obtained from Sigma) served as a control of functional activity. Arrow indicates position of EGFR. NIRF imaging with EGF/Cy of 4T1 tumor in Balb/c mice (bottom, left). Mice received i.v. 3.3 g Cys-EGF/Cy, which is a molar equivalent of scVEGF/Cy probe used for NIRF imaging (0.5 nmoles per mouse). Cy5.5 and CD31 co-localization analysis on 4T1 tumor cryosections (bottom, right). Cy5.5, red; CD31, green. Scale bar, 20 m.

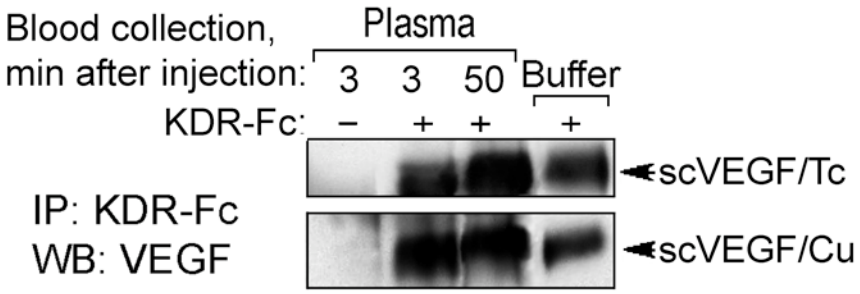
Blood collection,
min after injection:
Plasma
3
3
50
Buffer
KDR-Fc:
–
+
+
+
IP: KDR-Fc
WB: VEGF
scVEGF/Tc
scVEGF/Cu

Supplementary Figure 5. Stability of radionuclide-loaded scVEGF probes *in vivo*.
Soluble VEGF receptor KDR-Fc was collected on Protein A Sepharose from conditioned medium of 293/KDR-Fc cells as described[21]. 4T1luc tumor-bearing mice received i.v. either scVEGF/Tc (2.5 mCi/ 10 g per mouse, *n*=2) or scVEGF/Cu (36 Ci/ 6 g per mouse, *n*=2). We harvested blood 3 and 50 min after injections in sodium citrate Vacutainer tubes and centrifuged at 2,000X g for 15 min. Plasma aliquots containing equal amounts of radioactivity were mixed with sepharose-immobilized KDR-Fc to a molar KDR-Fc to scVEGF ratio of 2:1. For non-specific binding controls, plasma aliquots of 3-min blood samples were mixed with Protein A Sepharose without KDR-Fc. For electrophoretic mobility controls, radionuclide-loaded scVEGF probes were mixed with KDR-Fc in radiolabeling buffer (0.1 M NaOAc pH 5.5). After 1-h binding at 4 ºC, Sepharose beads were spun down, extensively washed with RIPA buffer, separated by reducing SDS-PAGE on 10% gels and analyzed by Western blotting with purified human VEGF-specific antibody (Pharmingen) diluted 1:2,000. Note that endogenous VEGF isoforms that might be precipitated with KDR-Fc from mouse blood migrate in reducing SDS-PAGE as monomers with apparent molecular weights of 16-18 kDa and therefore are readily separated from scVEGF/HYNIC (~29 kDa) and scVEGF-PEG-DOTA (~32 kDa).

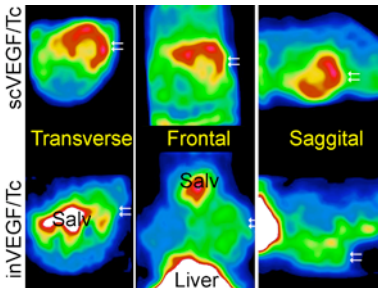
scVEGF/Tc
Transverse
Frontal
Saggital
inVEGF/Tc
Salv
Salv
Liver

Supplementary Figure 6. SPECT imaging of 4T1luc tumor bearing mice.
Representative transverse, frontal and sagittal SPECT images of two left axillary fat pad tumor bearing mice 1 h after intravenous injection of either scVEGF/Tc (top row) or inVEGF/Tc (bottom row). Note the peripheral rim uptake of scVEGF/Tc of tumor (double white arrows) as compared with inVEGF/Tc. Salv, uptake of trace free ^{99m}Tc in the salivary/neck region. Liver uptake was markedly higher (white is the highest activity in false color images) than tumor uptake of inVEGF/Tc. In order to satisfactory display both tumor and liver uptake in the same field of view, it was necessary to narrow the intensity window to a very low range resulting in a near white out of the salivary and liver regions.

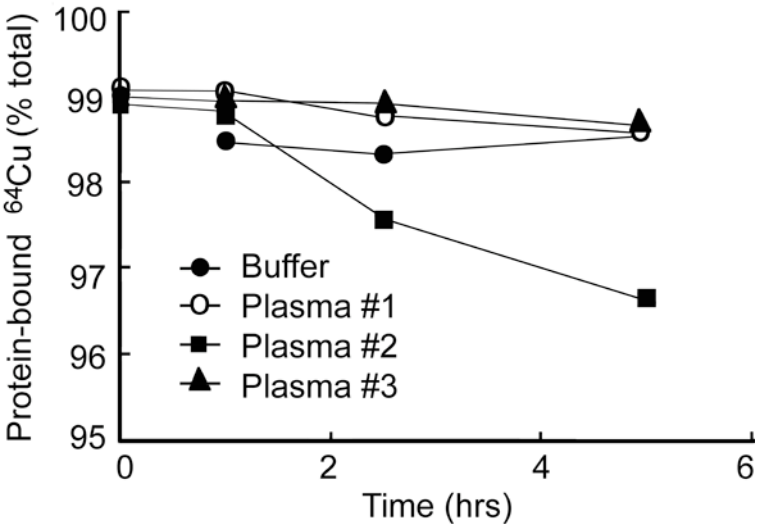
Protein-bound ^{64}Cu (% total)
100
99
98
97
96
95
0
2
4
6
Time (hrs)
Buffer
Plasma #1
Plasma #2
Plasma #3

Supplementary Figure 7. scVEGF/Cu stability in murine plasma *ex vivo*

Tumor-bearing mice (*n*=3) were injected i.v. with scVEGF/Cu (30 Ci, 3 g per mouse) and sacrificed 2 min later. Blood was collected and clarified by centrifugation as described in Legend to Supplementary Fig. 5. Plasma samples (#1-3) and equivalent amount of scVEGF/Cu in radiolabeling buffer (0.1 M NaOAc pH 5.5) were incubated at 37 ^{o}C. After 1, 2.5, and 5 h of incubation, free ^{64}Cu was separated by gel-filtration on PD-10 columns, and protein-bound ^{64}Cu was counted in a gamma-counter.